Adaptive Singularity Cancellation for Efficient Treatment of Near-Singular and Near-Hypersingular Integrals in Surface Integral Equation Formulations

Ismatullah and Thomas F. Eibert

***Abstract*—A recently proposed singularity cancellation technique for fully numerical evaluation of method of moments integrals in surface integral equation solutions produces reasonably accurate results with few quadrature points for singular and hypersingular integrals. However, for near-singular and near-hypersingular integrals, time-consuming computations need to be repeatedly performed over unnecessary regions outside the actual integration domain. For a more efficient treatment of these integrals, an adaptive singularity cancellation technique is proposed. As such, the source triangular domain is subdivided in a way that all sample points remain inside the desired integration domain and unnecessary computations are avoided. Second the accuracy of results in existing singularity cancellation transformations is greatly affected by variations in height of observation point above the plane of source domain. This drawback has been removed in the adaptive singularity cancellation transformations. Additionally, an optimum selection criterion for the distribution of quadrature samples is presented. The criterion enables run-time selection of optimum number of samples in different directions by consideration of the instantaneous geometry of the transformed integration domain.**

***Index Terms*—Integral equations, method of moments (MoM), singular integrals.**

I. Introduction

The accuracy of method of moments (MoM) solutions of integral equations depends significantly on the calculation of the coupling integrals, which involve singular kernels. Direct numerical quadrature is not applicable, especially for neighboring source and test domains, and special numerical treatment of such integrals is typically required.

Previously, the singularity subtraction and Duffy transformation methods [1] were often used for the evaluation of singular integrals. Most recently, singularity cancellation technique has come up for the treatment of singular integrals. In this technique, fully numerical evaluation of singular integrals has been proposed. For $1/R$–type singular kernels, *Arcsinh* transformation [2] transforms the source domain to a rectangular domain and cancels out the singularity. This rectangular transformed domain enables the integration over source domain with few sample points. For $\vec{R}/R^3$–type kernels, the Radial Angular-R^2 (RA-R^2) transformation [3] cancels out the singularity. However, the transformed domain is not rectangular and, depending upon the observed geometry of the source domain, often large numbers of Gauss-Legendre sample points are required for integration over the source domain. The singularity cancellation transformation appeared less efficient for near-singular and near-hypersingular couplings. The reason is that the observation point or the projection of observation point lies outside the source domain. In case of triangular domains, at least one of the subtriangles lies completely outside the source triangle and the remaining subtriangles are also partially outside. Thus, most of the sample points lie outside the required integration domain. The contribution of outer sample points is finally subtracted from the overall result. In order to avoid time-consuming integration over such sample points, we propose an adaptive singularity cancellation technique, which locates all sample points within the desired integration domain.

The convergence behavior of the existing singularity cancellation transformations is very sensitive to height of observation point above the plane of source domain. Often very large number of sample points are needed for existing schemes which badly degrades the computational efficiency. In [3], two different transformations were proposed to handle this problem. RA-R^2 was employed for higher values of $|z|$ and RA-R^3 was suggested for lower values of $|z|$. In fact this is not a preferable solution. However, the adaptive approaches produce accurate results with fewer quadrature points independent of the heights of observation point above the plane of source domain.

Another important feature for the improvement of efficiency is the appropriate choice of an adequate number of sample points according to the instantaneous shape of the transformed integration domain encountered during the analysis of a particular pair of source and test domains. Different numbers of sample points are chosen for different radial and angular dimensions of the transformed integration domain. For this, an optimum sample point distribution criterion is presented.

II. Review of Singularity Cancellation Transformations

The considered singular integrals encountered in surface integral equation formulations of radiation and scattering problems of arbitrarily shaped objects have the following general forms:

$$\boldsymbol{B} = \iint_{A'} \boldsymbol{\beta}(\boldsymbol{r}') \frac{e^{-jkR}}{R} da' \tag{1}$$

$$\boldsymbol{D} = \iint_{A'} \boldsymbol{\beta}(\boldsymbol{r}') \times \nabla \frac{e^{-jkR}}{R} da' \tag{2}$$

where $R = |\boldsymbol{r} - \boldsymbol{r}'|$, $\boldsymbol{\beta}$ is the vector basis function, and da' describes surface integral carried over the source or integration domain with area A'.

Now for the computation of singular integrals over triangular source domain, the original source domain is decomposed into three subtriangles all sharing the singular point (or its projection) as a common vertex. One of the edges of the original source domain belongs to one of the subtriangles. The x-axis of the coordinate system in a particular subtriangle is anti-parallel to the edge which belongs to the original source triangle, the y-axis is perpendicular to this edge and z-axis is outward normal to the source domain.

For $1/R$–type singular integral (1), the *Arcsinh* transformation is [2]

$$u = \mathrm{Arcsinh}\left(\frac{x}{\sqrt{y^2+z^2}}\right), \qquad v = y \tag{3}$$

where the integration domain is assumed to lie in the xy-plane with origin at the projected observation point (see Fig. 1 or [2]). The Jacobean of this transformation is R and cancels out the singularity and the integral (1) in the transformed domain becomes

$$\boldsymbol{B} = \int_{v_L}^{v_U} \int_{u_L}^{u_U} \boldsymbol{\beta}(\boldsymbol{r}')\, e^{-jkR} du\, dv \tag{4}$$

where $v_{L,U}$ and $u_{L,U}$ are the lower and upper limits of integration in the transformed domain. These limits are determined according to the geometry of the subtriangle under consideration. These limits of integration are given by

$$u_{L,U} = \mathrm{Arcsinh}\left(\frac{x_{L,U}}{\sqrt{y^2+z^2}}\right), \; v_{L,U} = y_{L,U} \tag{5}$$

Manuscript received January 31, 2007; revised September 1, 2007.

The authors are with the Institute of Radio Frequency Technology, Universität Stuttgart, Stuttgart D-70550, Germany (e-mail: eibert@ihf.uni-stuttgart.de).

Color versions of one or more of the figures in this paper are available online at http://ieeexplore.ieee.org.

Digital Object Identifier 10.1109/TAP.2007.913170

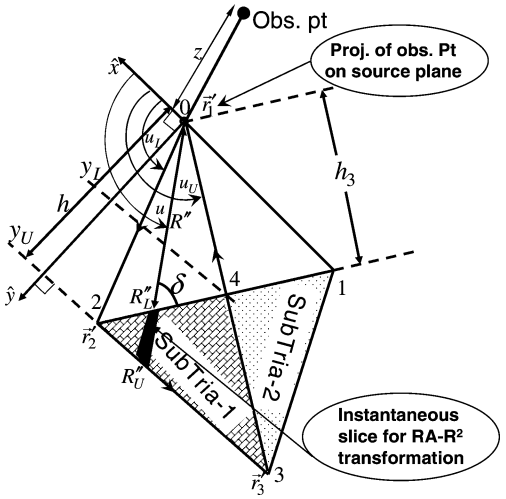

Fig. 1. Geometry and coordinate system of subtriangles in source domain, when one subtriangle is completely outside the original source domain $\Delta 123$.

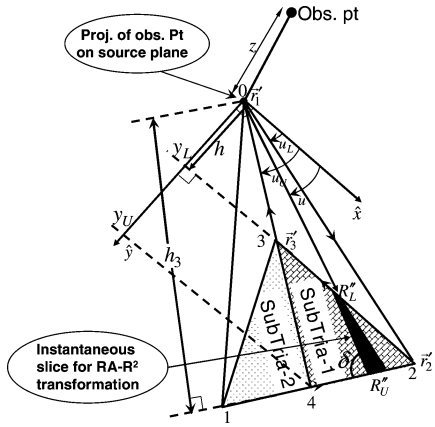

Fig. 2. Geometry and coordinate system of subtriangles in source domain, when two subtriangles are completely outside the original source domain $\Delta 123$.

where for existing scheme

$$y_{L,U} = 0, h \tag{6}$$

and h represents the height of projected observation point from the opposite edge of the subtriangle under consideration. In *Arcsinh* transformation, the transformed rectangular integration domain enables the use of Gauss-Legendre integration with very few sample points. Excellent convergence results are observed in this transformation.

For $\vec{R}/R^3$–type singular integral (2), the RA-R^2 transformation according to

$$u = \phi = \mathrm{Arctan}\left(\frac{y}{x}\right) \quad , \quad v = |z| \ln R \tag{7}$$

is considered [3]. The Jacobean of this transformation is $-(R^2/|z|)$, which cancels out the singularity. The limits of integration in the RA-R^2 transformation are given by

$$u_{L,U} = \phi_{L,U} \ , \ v_{L,U} = \frac{|z|}{2} \ln \left[z^2 + \left(R''_{L,U}(u) \right)^2 \right] \tag{8}$$

where for existing scheme

$$R''_{L,U}(u) = 0, \frac{h}{\sin(u)} \, . \tag{9}$$

The transformed integration domain in RA-R^2 transformation is not rectangular and is deformed as the observation point moves closer to the source or integration domain. Therefore, often very large numbers of sample points are necessary for sufficiently good accuracies.

In the following sections, we propose an adaptive approach for near-singular and near-hypersingular integrals while utilizing the benefits of the *Arcsinh* and the RA-R^2 singularity cancellation transformations.

III. Geometrical Configuration for Near-Singular Integrals

Dependent on the location of the projection of the observation point, two different geometrical configurations for near-singularities are possible, as shown in Figs. 1 and 2. The existing scheme divides the original triangle into three subtriangles and integration over all subtriangles starts from the origin (projection of observation point). As such, one subtriangle is completely outside the source domain for the geometry of Fig. 1, and two subtriangles are completely outside the source domain in the case of Fig. 2. It is noteworthy that any particular geometry of source and observation point can easily be categorized into either of these two cases from the knowledge of local normals of the three subtriangles.

In adaptive scheme, two out of three subtriangles of the existing scheme are taken into account, and limits of integration are modified in such a way that integration is carried out only in the regions of original source domain. The two subtriangles, SubTria-1 and SubTria-2, are shown shaded in Figs. 1 and 2. The adaptive limits of integration for RA-R^2 and *Arcsinh* transformations are described in the following paragraphs.

A. Adaptive Limits of Integration for Radial Angular-R^2 Transformation

In RA-R^2 transformation, the rectangular coordinate system (x, y) is transformed into angular and radial coordinates (u, v). The integration is carried out in transformed uv–domain. In the subtriangle under consideration, angular limits of integration $u_{L,U}$ are kept as in the existing scheme. However, the modified lower and upper limits in radial direction $R''_{L,U}$ for the computation of $v_{L,U}$ [see (8)] are given by

$$R''_{L,U}(u) = \frac{h_3}{\sin(\delta)}, \frac{h}{\sin(u)} \tag{10}$$

for the case of Fig. 1 and

$$R''_{L,U}(u) = \frac{h}{\sin(u)}, \frac{h_3}{\sin(\delta)} \tag{11}$$

for the case of Fig. 2.

Equations (10) and (11) represent the respective instantaneous radial distances. Here, h represents the perpendicular distance of projection of the observation point from the opposite edge ($|23|$ or $|31|$) in the subtriangle under consideration, h_3 is the perpendicular distance from the edge $|12|$ and δ is the angle of instantaneous radius vector R'' as measured with edge $|12|$ (Figs. 1 and 2).

B. Adaptive Limits of Integration for Arcsinh Transformation

For $1/R$-type singularities, the lower and upper limits $x_{L,U}$ and $y_{L,U}$ in the *Arcsinh* transformation are constrained by the sides of the subtriangle under consideration. These limits are used in the computation of integration limits [see (5)] and can be determined from the intersection of appropriate straight lines which bound the subtriangle under consideration. For the geometry of Fig. 1, the integration limits are given by

$$y_{L,U} = m_2 \left(\frac{y_1 - m_1 x_1}{m_2 - m_1} \right), \ h \tag{12}$$

$$x_{L,U}(y) = \frac{y}{m_2},\ \frac{y - y_1 + m_1 x_1}{m_1}. \tag{13}$$

Similarly, for the geometry of Fig. 2, the integration limits are given by

$$y_{L,U} = h,\ m_2\left(\frac{y_1 - m_1 x_1}{m_2 - m_1}\right) \tag{14}$$

$$x_{L,U}(y) = \frac{y - y_1 + m_1 x_1}{m_1},\ \frac{y}{m_2} \tag{15}$$

where

$$m_1 = \frac{y_2 - y_1}{x_2 - x_1} \quad \text{and} \quad m_2 = \frac{y_3}{x_3} \tag{16}$$

are the slopes of the two sides of the source triangle.

IV. Adaptive Criterion for Distribution of Sample Points

The selection of the number of sample points in the transformed non-rectangular domain is of critical nature. The deformation in the transformed domain becomes more and more pronounced as the projected observation point moves closer to the boundary of the original source domain and a larger number of sample points is needed to achieve accurate results. Also, it is observed that the integrands exhibit larger variations when the size of the integration domain relative to its distance from the projection of the observation point becomes larger. Therefore, a real-time selection of distribution of sample points for the particular geometry encountered is employed in order to account for the particular deformations and integrand variations and to enhance the efficiency of the solver to a great extent.

As in the existing schemes, the Gaussian quadrature rule is applied and the number of sample points is selected proportional to the observed relative angular and radial dimensions (with respect to the observation point or its projection) of the instantaneous slice of the subtriangle under consideration. The instantaneous check on the ratio of the length of the slice to its radial proximity from the projection of the observation point enables the use of optimum numbers of sample points.

The parameters $\alpha_\phi = |(\phi_U - \phi_L)/\pi|$ and $\alpha_R = |(R_U'' - R_L'')/R_U''|$ are proposed for the adaptive selection criterion in the angular and radial directions, respectively. For smaller angular dimensions, described by smaller values of α_ϕ, as few as two sample points are sufficient (assuming linear vector basis functions), whereas for larger angular dimensions, described by larger values of α_ϕ, more sample points are required for good accuracies. Similarly, more sample points are required for larger values of α_R. Although the number of sample points in a particular radial or angular segment are proportional to $\alpha_{R,\phi}$, yet, the exact numbers depend on the desired accuracy and can be determined from the numerical experiments. For our requirements, we have subdivided the complete range of $\alpha_{R,\phi} \in [0, 1]$ into four segments and used different number of samples for different segments.

In order to demonstrate the adaptive selection of the number of sample points in radial and angular directions, in Fig. 3 a fixed source domain is shown for two different observation points. In Fig. 3(a), as seen from the observation point, the angular domain of the right-sided subtriangle is larger than that of the left-sided subtriangle. Therefore, the adaptive scheme chooses eight samples in angular direction for the right-sided subtriangle and two angular samples for the left-sided subtriangle. Moreover, because the instantaneous slices are not very broad in the radial direction, only two sample points in radial direction are chosen. However, in Fig. 3(b) the angular domain as observed from the observation point is very small and, therefore, only two angular samples are chosen. Since each instantaneous radial slice is of significantly different size, the adaptive scheme chooses more samples (i.e., eight) for the larger slice and less sample points (i.e., 2) for the smaller slice.

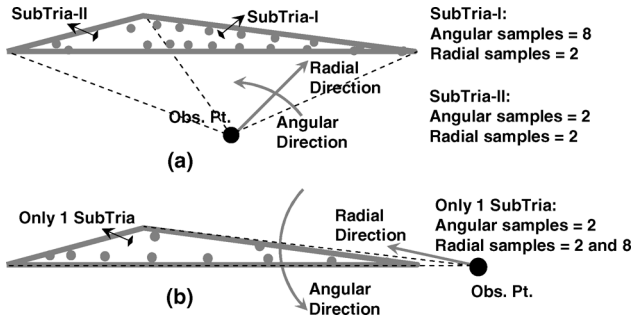

Fig. 3. Adaptive distribution of Gauss-Legendre sample points for a fixed source domain and two different observation points.

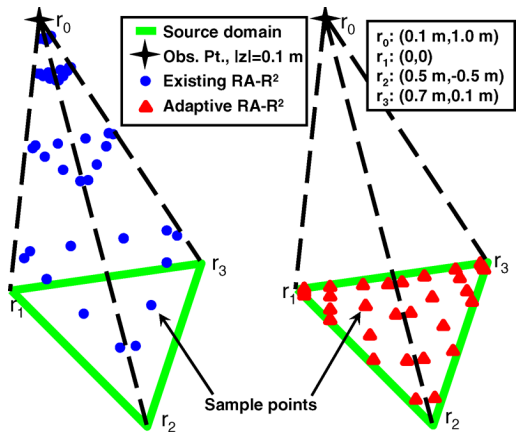

Fig. 4. Comparison of distribution of Gauss-Legendre sample points for a near-singularity in the existing and adaptive RA-R^2 transformations.

V. Numerical Results

A comparison of distribution of Gauss–Legendre sample points in the existing and adaptive RA-R^2 singularity cancellation transformations is shown in Fig. 4. It can be observed that for 4×4 distribution of sample points per subtriangle, the existing scheme uses a total of $4 \times 4 \times 3 = 48$ points in the source triangle, out of which only few are located within the desired source subdomain. However, the proposed scheme utilizes $4 \times 4 \times 2 = 32$ points, all of which are located completely inside the source subdomain. This enables the computation of accurate results with fewer sample points. In the subsequent results, the real part of the potential integral (1) with scalar basis function for *Arcsinh* and real part of the normal component of (2) with Rao–Wilton–Glission vector basis functions for RA-R^2 were computed at 10 m wavelength. In Fig. 5, the convergence of the existing and adaptive schemes is presented for the calculation of potential gradient integral (2). The proposed scheme converges for a total of $2 \times 2 \times 2 = 8$ sample points, whereas the existing scheme is approximately converged with $5 \times 5 \times 3 = 75$ sample points.

In Fig. 6, we consider a special case in which the source domain is highly deformed. The integral (2) was computed using the existing and adaptive RA-R^2 schemes. The adaptive scheme is remarkably faster than the existing one.

In another example, we consider a right triangular source domain with vertices (0, 0, 0), (1 m, 0, 0), and (0, 1 m, 0). The observation point is taken at ($-$ 0.1 m, 0.1 m, 0.01 m). A comparison of convergence behavior in existing and adaptive *Arcsinh* transformations is presented in Fig. 7. The highly efficient converging behavior of the adaptive *Arcsinh* transformation is self evident. Similar to RA-R^2, the adaptive *Arcsinh* scheme converges rapidly even for highly deformed geometries. Another interesting benefit of the adaptive scheme over the

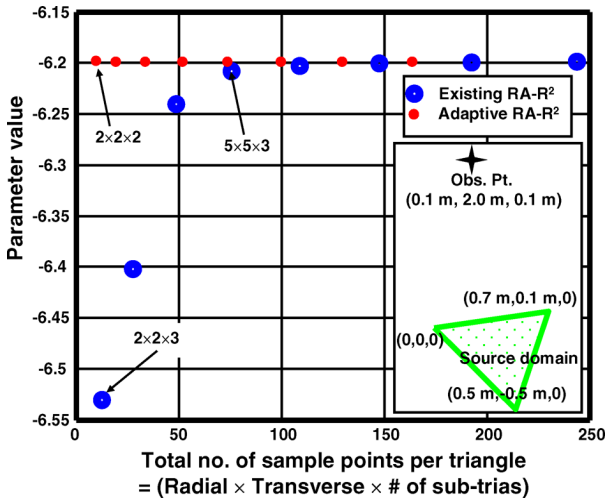

Fig. 5. Convergence results of a near-singularity in the existing and adaptive RA-R^2 transformations for the computation of (2) over the source domain shown in the lower legend.

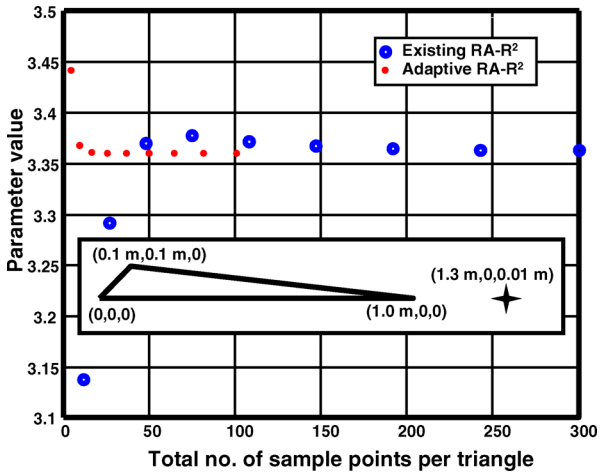

Fig. 6. Convergence results of the existing and adaptive RA-R^2 transformations for the computation of (2) over a degenerate source domain shown in the lower legend.

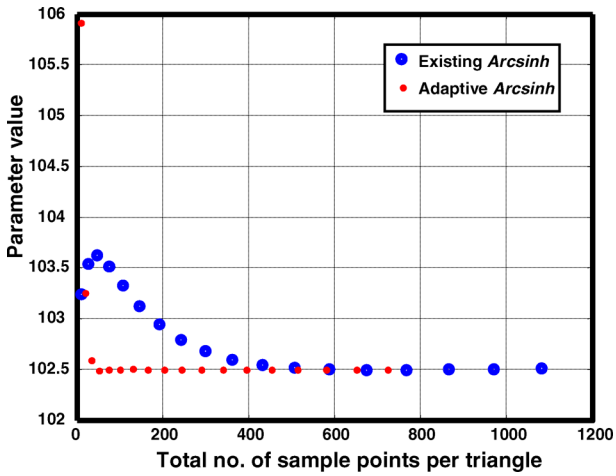

Fig. 7. Convergence results of a near-singularity in the existing and adaptive *Arcsinh* transformations for the computation of (1).

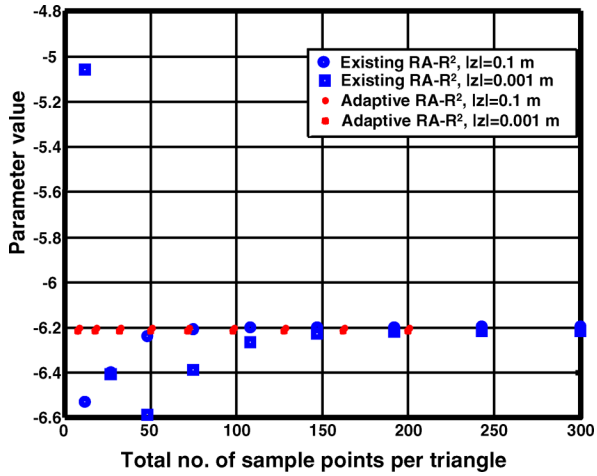

Fig. 8. Comparison of convergence behavior of existing and adaptive RA-R^2 transformations for different heights $|z|$ of observation point over the source domain for the computation of potential gradient integral (2).

existing scheme is that it converges rapidly independent of height of observation point above the plane of source domain. For this purpose, the geometry being used has the vertices (0, 0, 0), (0.5 m, -0.5 m, 0) and (0.7 m, 0.1 m, 0). The near-singular observation point is located at (0.1 m, 2.0 m, $|z|$). A comparison of convergence behaviors of existing and adaptive RA-R^2 schemes for two different heights $|z| = 0.1$ m, 0.001 m, is presented in Fig. 8. This shows that the convergence behavior of existing RA-R^2 transformations is highly sensitive to the height $|z|$ of the observation point above the source plane. The sensitivity to z-variations of the existing RA-R^2 scheme is due to the fact that as the height of observation point above the source plane is decreased, the quadrature points start clustering more closer to the observation point. Since for near-singularities, the observation point resides outside the actual source domain, the number of samples which are inside the original source domain are reduced and hence the accuracy of the computation becomes worse. However, this is not the case for the proposed adaptive transformations. Because all of the quadrature points already reside completely inside the original source domain, therefore the adaptive version of the transformation converges with fewer sample points regardless of the height of the observation point over source plane. Similarly the convergence of adaptive *Arcsinh* scheme has been found independent of z-variations in the observation point.

Finally, a comparison of the computational efficiencies of existing and adaptive schemes was carried out under the same memory and speed environments for the computation of the near field matrix for a problem with 135876 unknowns. For a comparable accuracy of the order of two significant digits, the existing scheme took 2926 seconds whereas the adaptive scheme took 606 seconds. This explains the effectiveness of the adaptive scheme over the existing scheme.

VI. Conclusion

An adaptive singularity cancellation scheme for *Arcsinh* and RA-R^2 transformations was proposed for the efficient computation of near- and near-hyper-singularities for triangular domains. In the existing singularity cancellation approaches, the Gauss–Legendre quadrature points are clustered around the observation point or its projection and therefore often a large number of sample points for sufficiently good accuracies are needed. Highly efficient treatment of these cases has been proposed by retaining all the quadrature points completely inside the desired integration domain. Also, the adaptive *Arcsinh* and RA-R^2 transformations are insensitive to z-variations of the observation point.

Therefore, very few sample points are needed for sufficiently good accuracies for near-singular and near-hypersingular kernels of potential integrals. Also, an optimum criterion for the distribution of sample points in two directions was found proportional to the radial and angular dimensions of the instantaneous slices of the source domain.

ACKNOWLEDGMENT

This work was carried out at the Institute of Radio Frequency Technology (IHF), Universität Stuttgart, Stuttgart, Germany under the collaborative Ph.D. scholarship scheme between the Higher Education Commission of Pakistan (HEC) and the Deutscher Akademischer Austausch Dienst (DAAD).

REFERENCES

[1] M. G. Duffy, "Quadrature over a pyramid or cube of integrands with a singularity," *SIAM J. Numer. Anal.*, vol. 19, no. 6, pp. 1260–1262, Dec. 1982.

[2] M. A. Khayat and D. R. Wilton, "Numerical evaluation of singular and near-singular potential integrals," *IEEE Trans. Antennas Propag.*, vol. 53, pp. 3180–3190, Oct. 2005.

[3] P. W. Fink, D. R. Wilton, and M. A. Khayat, "Issues and methods concerning the evaluation of hypersingular and near-hypersingular integrals in BEM formulations," presented at the Int. Conf. on Electromagnetics in Advanced Applications (ICEAA), Turin, Italy, Sep. 12–16, 2005.

Implementation of Method of Moments for Numerical Analysis of Corrugated Surfaces With Impedance Boundary Condition

Ilari Hänninen and Keijo Nikoskinen

***Abstract*—A method of moments formulation is developed to analyze the scattering of corrugated surfaces by using an impedance boundary condition. The numerical analysis of the impedance surface is done using closed-form formulae and accurate numerical integration. The studied formulation greatly decreases the computational resources required to study corrugated structures.**

***Index Terms*—Corrugated surface, method of moments (MoM), radar cross section (RCS).**

I. INTRODUCTION

Corrugated surfaces pose challenging problems regarding numerical computations. They are constructed—in terms of wavelength—of very thin grooves, that require a very fine mesh to model, which in turn leads to high memory requirements and long computation times. On the other hand, corrugation is usually used in situations where the corrugation is quite uniform and continuous on a relatively large surface area. Thus the small-scale effects on the scattering response of the individual grooves are usually masked by the large-scale effects of the corrugated surface as a whole. If one were able to replace the corrugation in the numerical model by a surface that has the same large-scale effects as the corrugated surface but which is smooth, i.e., without grooves, one could diminish the high computational cost considerably.

Manuscript received February 2, 2007; revised September 1, 2007.

The authors are with the Electromagnetics Laboratory, Helsinki University of Technology, FI-02150 Espoo, Finland (e-mail: ilari.hanninen@tkk.fi).

Digital Object Identifier 10.1109/TAP.2007.913171

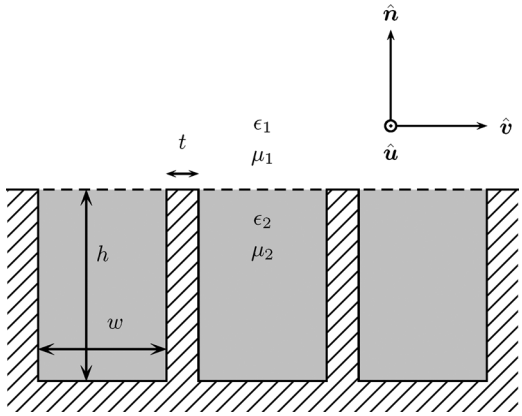

Fig. 1. Geometry and the physical properties of the corrugation.

In this Communication, the authors introduce a method of moments (MoM) implementation which exploits the impedance boundary condition (IBC) in numerical analysis of the corrugation. The method proposed treats the grooves of the corrugation as short-circuited waveguides, which enables one to compute the impedance values analytically. Previously, a method applying the soft-and-hard surface (SHS) [1], [2] boundary approximation was suggested for the computational analysis of corrugated surfaces [3]. However, the SHS approximation is valid only for a single frequency whereas the IBC can be used to compute the scattering response of the corrugated surface for a frequency band around and including the SHS case. Asymptotic boundary conditions (ABC) have also been used to model corrugations with good success [4]–[6]. The IBC method was chosen in this paper because it is simple, easy to implement, and reduces the number of unknowns significantly. The IBC is used with a surface integral equation method to solve the scattered field numerically, using MoM. The results produced by this method are compared to the numerical analysis of the exact model of the corrugation by *CST Microwave Studio* using finite integration technique (FIT).

II. IMPEDANCE BOUNDARY CONDITION FOR CORRUGATED SURFACE

Let us consider a corrugated surface that is sufficiently smooth so that it can be locally approximated by a flat surface. We will denote the direction of the corrugation by $\boldsymbol{u}$ and the direction perpendicular to the corrugation by $\boldsymbol{v}$, so that $\boldsymbol{u} \times \boldsymbol{v} = \boldsymbol{n}$, where $\boldsymbol{n}$ is the unit normal vector to the surface (see Fig. 1). A corrugated surface can be approximated, within certain limitations, by the impedance boundary condition

$$\boldsymbol{E}_t(\boldsymbol{r}) = \overline{\boldsymbol{Z}}_s \cdot \boldsymbol{n}(\boldsymbol{r}) \times \boldsymbol{H}_t(\boldsymbol{r}) \tag{1}$$

where $\boldsymbol{E}_t$ and $\boldsymbol{H}_t$ are the field components tangential to the surface, and $\overline{\boldsymbol{Z}}_s$ is the surface impedance dyadic

$$\overline{\boldsymbol{Z}}_s = Z_u \boldsymbol{u}\boldsymbol{u} + Z_v \boldsymbol{v}\boldsymbol{v}. \tag{2}$$

We can also write the impedance boundary condition by means of the surface admittance dyadic $\overline{\boldsymbol{A}}_s = \overline{\boldsymbol{Z}}_s^{-1}$ as

$$\boldsymbol{H}_t(\boldsymbol{r}) = -\overline{\boldsymbol{A}}_s \cdot \boldsymbol{n}(\boldsymbol{r}) \times \boldsymbol{E}_t(\boldsymbol{r}). \tag{3}$$

The impedance values Z_u and Z_v in (2) can be computed by approximating the grooves of the corrugation by short-circuited wave guides if the width of the grooves is sufficiently small, and the values are given by [3]

$$Z_u = iZ^{\mathrm{TE}_1} \tan(\beta^{\mathrm{TE}_1} h), \quad Z_v = i\eta_2 \tan(k_{2n} h) \tag{4}$$